Laser nanotrapping and manipulation of nanoscale objects using subwavelength apertured plasmonic media

Alexander Baev, Edward P. Furlani, Paras N. Prasad, Alexander N. Grigorenko, and Nicholas W. Roberts

Citation: Journal of Applied Physics **103**, 084316 (2008); doi: 10.1063/1.2912493
View online: http://dx.doi.org/10.1063/1.2912493
View Table of Contents: http://scitation.aip.org/content/aip/journal/jap/103/8?ver=pdfcov
Published by the AIP Publishing

Laser nanotrapping and manipulation of nanoscale objects using subwavelength apertured plasmonic media

Alexander Baev,[1,a)] Edward P. Furlani,[1] Paras N. Prasad,[1,b)] Alexander N. Grigorenko,[2] and Nicholas W. Roberts[2]
[1]*The Institute for Lasers, Photonics and Biophotonics, State University of New York at Buffalo, Buffalo, New York 14260-3000, USA*
[2]*School of Physics and Astronomy, University of Manchester, Manchester M13 9PL, United Kingdom*

(Received 3 December 2007; accepted 27 February 2008; published online 29 April 2008)

We study the net radiation force on dielectric nanowires above a planar plasmonic medium consisting of a nanostructured gold film on a glass substrate. The film has a subwavelength aperture and the medium is illuminated by a continuous plane wave. We compute the steady-state field distribution by using two-dimensional finite element analysis, and we evaluate the force on the nanowires above the aperture by using the Maxwell stress tensor. We show that the vertical position of a nanowire can be controlled by either tuning the wavelength of the laser source or tapering the aperture. We experimentally check the conclusions of the theory by realizing laser nanotrapping of dielectric beads near the surface of nanostructured metal. Our results demonstrate the potential of using nanostructured plasmonic media for the controlled optical manipulation of nanowires and nanoparticles, including their application as "plasmonic sieve" for separation based on size and/or refractive index. © *2008 American Institute of Physics*. [DOI: 10.1063/1.2912493]

I. INTRODUCTION

The ability to control the interaction of light and matter at the nanoscale has enabled fundamental advances across a broad range of applications at the intersection of diverse fields such as spectroscopy, lithography, and biosensing.[1] In this paper, we study the optical trapping and manipulation of nanoparticles, which holds potential for applications in nanoparticle chemistry, nanorheology, and ultrasensitive biosensors.[2–7] Submicron particles can be positioned by using conventional (far-field) optical tweezers, but the trapping volume of this approach is limited by the diffraction limit (~250 nm) of the optics used to produce the spatial gradient of light required to trap a dielectric particle (plasmonic particles of much smaller sizes, such as 18 nm gold particles, can be nevertheless trapped by making use of far-field tweezers[8]). Nanopositioning by using conventional optical tweezers is still possible, but it requires high laser powers, which could be damaging to bio-objects or special nanoparticles with high polarizabilities. It is known, however, that small particles can be manipulated and trapped at relatively small trapping powers by using the enhanced near-field gradients that exist around subwavelength apertures in thin metallic films or subwavelength plasmonic islands on dielectric substrates[9–22] (interested readers are referred to a review article[23] for more experimental details). While other authors studied near-field effects on particles, a relatively few studies (see, e.g., Ref. 21) have focused on two-dimensional (2D) or three-dimensional (3D) controlled manipulation, i.e., particle trapping/release. Moreover, in this paper, we use a dipolar force potential to analyze the 2D force distribution,[12,21] whereas most of the other works reduce to a one-dimensional Maxwell stress tensor analysis of the attractive/repulsive force along one coordinate direction.

We study the optical manipulation of dielectric nanowires above a planar plasmonic medium consisting of a thin gold film on a glass substrate in air (Fig. 1). The film has a subwavelength slit aperture, and the medium is illuminated by a continuous plane wave (cw) source positioned beneath the substrate. The thicknesses of the film and the substrate are 100 nm and 1 μm, respectively, and the wavelength of the incident radiation is 400 nm. The substrate (silica glass) has a refractive index of 1.45 and is considered transparent to the incident light. The dielectric permittivity of the gold film is chosen to be Drude type with the following parameters:

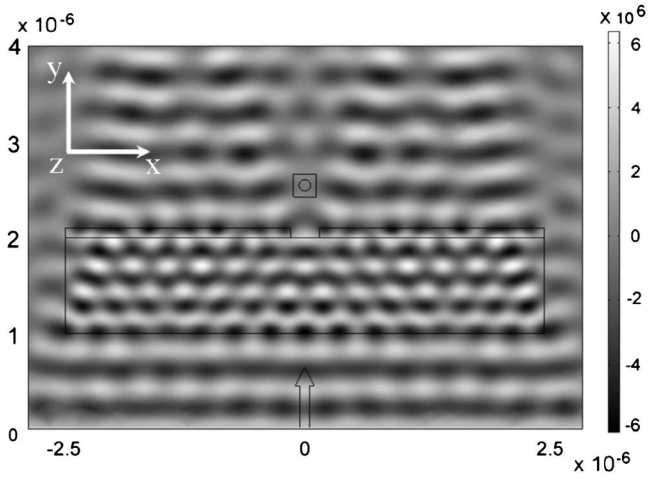

FIG. 1. Map of the Z-component of the electric field. The black lines show the film, the slit, the substrate, and the wire. The wire with the radius of 60 nm is at 400 nm above the surface of the substrate. The arrow indicates the direction of light propagation.

[a)]Electronic mail: abaev@buffalo.edu.
[b)]Author to whom correspondence should be addressed. Electronic mail: pnprasad@buffalo.edu.

the bulk plasma frequency is 1.37×10^{16} s^{-1}, the damping frequency is 4.08×10^{13} s^{-1}, and the high-frequency limit term including contributions from interband transitions is 12.9. It is important to note that while other studies[8] were performed by using an opaque perfectly conducting layer with an aperture, we instead use a Drude permittivity to model the metallic film, which gives rise to important features of near-field trapping that are not manifested in the perfectly conducting layer analysis. These effects include a wavelength dependence of the force and a spatial change in the sign of the force, which is a key characteristic of trapping. We would also like to note that the Drude model may not provide accurate results in the visible and UV range of wavelengths.[24] To circumvent this problem, one can fit the permittivity within the range of interest by modifying the values of the parameters of the Drude model. The set of parameters used in our simulations were optimized for the visible range.

II. METHODOLOGY

We analyze a medium/nanowire system by using 2D finite element analysis (FEA), which is implemented by using the COMSOL FEMLAB software.[25] We impose perfectly matched layer (or low-reflecting) boundary conditions on all passive external boundaries. We compute the time-averaged electromagnetic force on a nanowire by using the Maxwell stress tensor,

$$\overleftrightarrow{T}_{ij} = E_i D_j + B_i H_j - \tfrac{1}{2}(\vec{E}\cdot\vec{D} + \vec{B}\cdot\vec{H})\delta_{ij}, \tag{1}$$

where δ_{ij} is the Kronecker delta function. Specifically,

$$\vec{F}_{em} = \left\langle \oint_A (\overleftrightarrow{T}\cdot\hat{n})dA \right\rangle, \tag{2}$$

where $\langle\cdots\rangle$ represents a time average and $\hat{n}$ is the unit normal to the surface A, which encloses the wire. In the 2D FEA, we choose a rectangular surface that encloses only the nanowire; the substrate, film, and source are outside this region. We study the system by using TE analysis (transverse electric plane wave, the electric field is polarized along z-axis). It is worth noting that the force can also be computed by using finite difference time domain (FDTD) analysis for the field solution and a Poynting vector approach for the force.[26–28] However, as correctly pointed out in Ref. 29, this approach works only in the case when the normal to the surface element and direction of energy flow, passing through this surface element, are parallel. Moreover, there are technical issues with achieving a stable steady-state field solution using the FDTD approach, which complicates the force analysis. The source is a cw, which propagates upward (y direction) from the lower boundary of the FEA solution space. The electric field strength on this boundary is set to 3×10^6 V/m, which corresponds to a cw power per unit length of 72 mW/μm.

III. RESULTS AND DISCUSSION

We study the vertical optical force $F_{em,y}$ on a dielectric nanowire with a radius $a=60$ nm and a refractive index of 1.3. We compute this force as a function of both the distance y above the substrate, $y=200-900$ nm, and the width (d) of the aperture, $d=200$, 250, and 300 nm (Fig. 2). We find that for each width d, there are two equilibrium positions where $F_{em,y}=0$. Specifically, the equilibrium positions are $y=260$ and 633 nm for $d=200$ nm, $y=263$ and 643 nm for $d=250$ nm, and $y=261.5$ and 671 nm for $d=300$ nm. Note that if the wire is vertically displaced about these points, the optical force acts to restore the wire to the equilibrium position, i.e., positive vertical displacements result in negative values of force, whereas negative vertical displacements result in positive values of the force. Next, we examine the lateral optical force $F_{em,x}$ around the two equilibrium points for the 300 nm wide aperture (Fig. 3). The analysis indicates that only one of the points, specifically $y=671$ nm, is a lateral equilibrium point, as $F_{em,x}$ acts to restore the wire to this point upon small lateral displacements. In order to determine

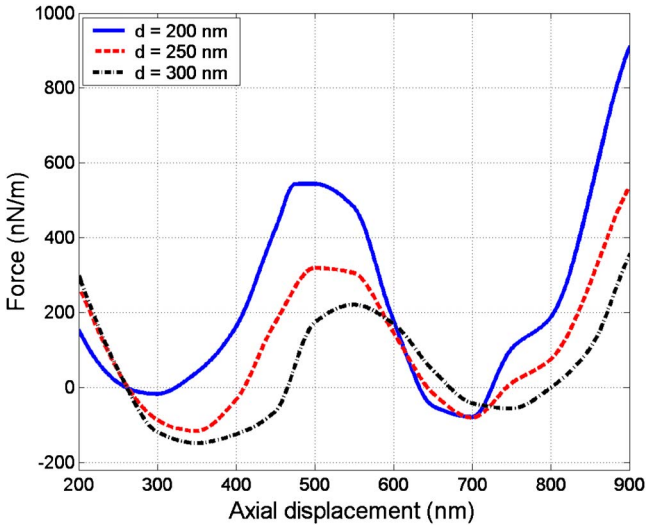

FIG. 2. (Color online) Axial net radiation force vs axial displacement for a 60 nm radius dielectric wire ($n=1.3$) illuminated by 400 nm TE cw laser source.

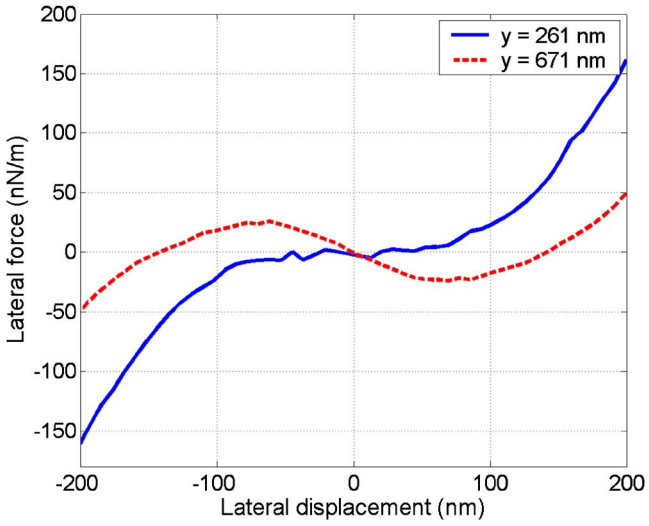

FIG. 3. (Color online) Lateral net radiation force vs lateral displacement for a 60 nm radius dielectric wire ($n=1.3$) illuminated by 400 nm TE cw laser source through a 300 nm wide rectangular slit.

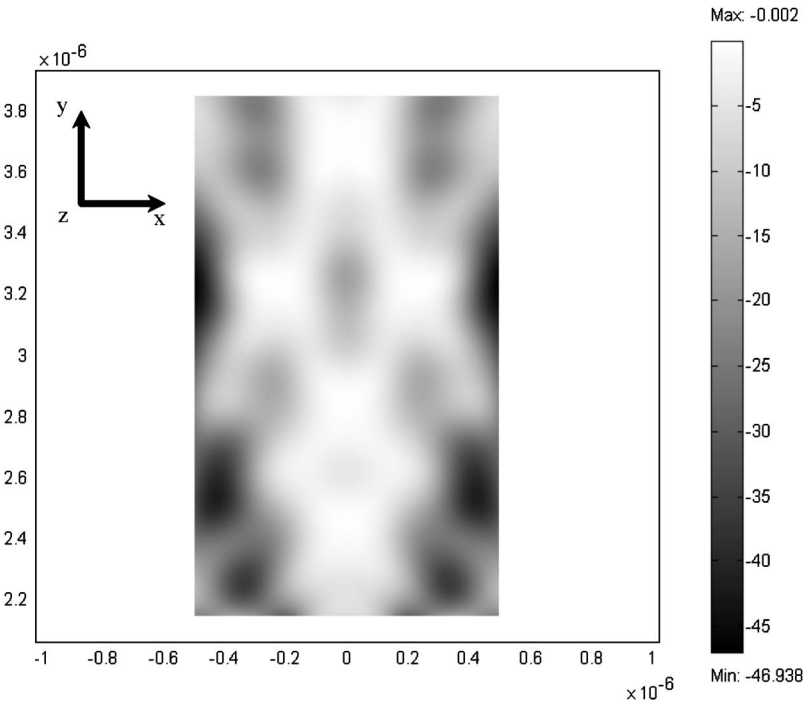

FIG. 4. Map of potential for the dipolar force. The units of x and y are meters.

if the wire is trapped at this point, we need to examine the force on the wire for any displacement. To this end, we apply a dipolar approximation ($a \ll \lambda$) and study the time-averaged force on the wire in the time-harmonic field above the aperture. In our 2D TE FEA, the force components on the wire at a position $\mathbf{r}$ reduce to[12] (in SI units)

$$F_x(\mathbf{r}) = \frac{\varepsilon_0}{2}\mathrm{Re}\{\alpha E_z(\mathbf{r})\partial_x[E_z(\mathbf{r})]^*\} \tag{3}$$

and

$$F_y(\mathbf{r}) = \frac{\varepsilon_0}{2}\mathrm{Re}\{\alpha E_z(\mathbf{r})\partial_y[E_z(\mathbf{r})]^*\}, \tag{4}$$

where α is the polarizability of the wire,

$$\alpha(\omega) = \frac{\alpha_0(\omega)}{1 - \frac{1}{2}ik^2\pi\alpha_0(\omega)}, \tag{5}$$

and

$$\alpha_0(\omega) = \frac{a^2}{2}\left[\frac{\varepsilon(\omega) - 1}{\varepsilon(\omega) + 2}\right], \tag{6}$$

where $\varepsilon(\omega) = \varepsilon_p(\omega)/\varepsilon_m(\omega)$ is the ratio of the permittivities of the wire and surrounding medium. In Eqs. (3) and (4), the field E_z is computed with the wire absent, i.e., the dipolar analysis does not take into account the effect of the particle on the field. We compute the potential $U(\mathbf{r})$ for the dipolar force,

$$U(\mathbf{r}) = -\frac{\varepsilon_0}{2}\mathrm{Re}\{\alpha E_z(\mathbf{r})[E_z(\mathbf{r})]^*\}, \tag{7}$$

for the medium with a 300 nm wide slit in Fig. 4 (in arbitrary units). From this analysis, we find that the equilibrium point $y = 671$ nm is a local minimum of $U(\mathbf{r})$, which indicates trapping, as small displacements in any direction about this point result in a restoring force back toward the point. Similar results are obtained with the other aperture widths: $d = 200$ and 250 nm.

To ensure that a particle is trapped at a point, the optical restoring force needs to be greater than the gravitational and Brownian/Langevin forces. For the example above, the gravitational force is more than the order of magnitude and less than the peak optical restoring force, and this is true for all of the examples considered in this paper. The Langevin force, which describes the random force on a particle in a fluid, depends on the viscosity and temperature of the fluid, as well as the time interval of measurement. We calculate this force to be approximately 0.6 nN/m for a wire with a radius of 60 nm in air at $T = 300$ °C when the measurement period is 1 s. Even when the particles are in water, the Langevin force is approximately 4 nN/m, which is still much smaller than the optical trapping force. Thus, aqueous environments, which are typically used for experiments with biological agents, are suitable for optical nanotrapping measurements.

It is instructive to compare this plasmonic aperture based particle trapping to conventional laser tweezer trapping. In laser trapping, the net radiation force on a particle can be decomposed into two components (Rayleigh approximation): a gradient force and a scattering force. The gradient (pulling) force, which results from the field gradient in the focused laser beam, competes with the scattering (pushing) force, giving rise to a single trapping position. However, in aperture based near-field trapping, the diffraction of the plane wave through the aperture creates a complex diffraction pattern with multiple trapping points, as seen in Fig. 4.

Next, we study the optical force as a function of wire radii $a = 30$, 60, and 100 nm for a fixed slit width $d = 300$ nm. The analysis indicates that the wires have poten-

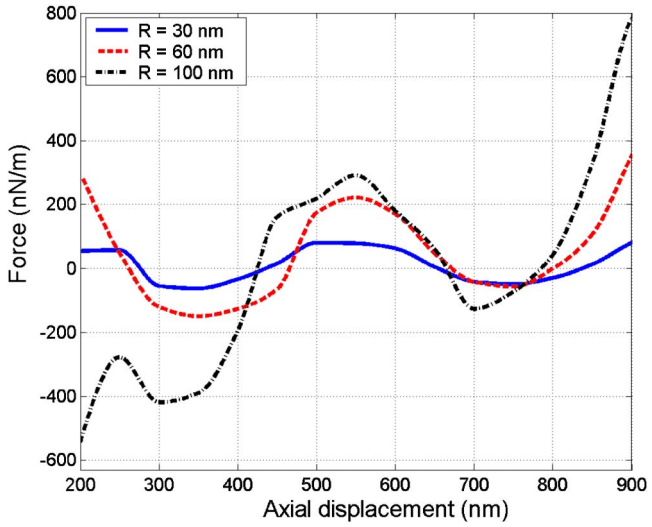

FIG. 5. (Color online) Axial net radiation force vs axial displacement for a dielectric wire ($n=1.3$) illuminated by 400 nm TE cw laser source through a 300 nm wide rectangular slit.

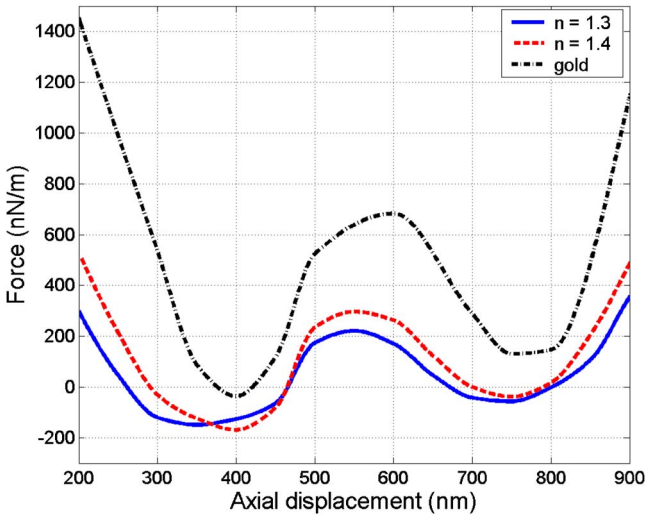

FIG. 7. (Color online) Axial net radiation force vs axial displacement for a 60 nm radius wire illuminated by 400 nm TE cw laser source through a 300 nm wide rectangular slit.

tial trapping points at different distances from the substrate, i.e., $y=653$, 671, and 665 nm, respectively (Fig. 5). These differences are due to the fact that differently sized nanowires perturb the incident field to different degrees. Thus, it may be possible to optically separate or sort nanowires with different radii, thereby creating a "plasmonic sieve."

The wavelength dependence of the optical force is presented in Fig. 6. Specifically, we study the force on a 60 nm nanowire for $\lambda=400$, 500, and 600 nm. Note that the magnitude of the force dramatically increases when $\lambda=500$ nm, which is around the resonant wavelength, λ_{res}, of the Drude permittivity of the film. At this wavelength, the film becomes essentially opaque to the incident field. Therefore, the restricted transmission/diffraction through the aperture produces a much larger field gradient as compared to the other wavelengths for which the film is partially transparent. Furthermore, while the optical force is strictly repulsive at $\lambda=500$ nm, it can be either positive or negative at other wavelengths, depending on the position of the nanowire. It is instructive to note that the slope ($\partial_y F_{em,y}$) of the force versus distance curve $F_{em,y}(y)$ depends on the magnitude of λ relative to λ_{res}. Specifically, the sign of this slope above λ_{res} ($\lambda=600$ nm) is opposite to that below ($\lambda=400$ nm). Moreover, the sign of the slopes are such that the nanowire can be trapped above the aperture when $\lambda=400$ nm, but not at $\lambda=600$ nm. From this analysis, we find that a nanowire can be potentially trapped or released by tuning the wavelength.

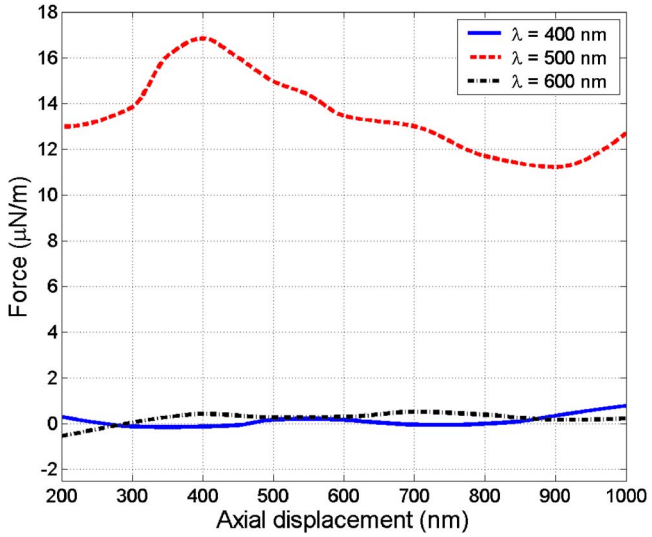

FIG. 6. (Color online) Axial net radiation force vs axial displacement for a 60 nm radius dielectric wire ($n=1.3$) illuminated by a TE cw laser source through a 300 nm wide rectangular slit.

Next, we study the optical force as a function of the nanowire dielectric properties. We study three cases: $n=1.3$, $n=1.4$, and a gold plasmonic wire. The results are presented in Fig. 7. From this analysis, we find that there are multiple equilibrium positions for the two dielectric wires and that these positions depend on the refractive index n. Thus, it is potentially possible to optically separate such wires. However, the plasmonic wire differently responds; there is only a single equilibrium position and the (negative) optical force above this position is relatively weak. Thus, the optical "trapping" power needs to be significantly higher for the plasmonic wire (as compared to the dielectric wires) to preclude Brownian diffusion away from the equilibrium position.

We also investigate the dependence of the optical force on the shape of the aperture. Specifically, we consider a tapered slit with the lower spacing of 300 nm and two different upper spacings: 100 and 200 nm, respectively. The force profiles for these geometries are shown in Fig. 8. We find that the shape of the aperture affects the equilibrium position of the wire as well as the height of the positive and negative force barriers.

IV. EXPERIMENTAL REALIZATION OF NANOTWEEZERS

Finally, we describe an experimental realization of laser nanotweezers based on nanostructured substrates. We use the standard laser tweezer setup shown in Fig. 9(a). The laser

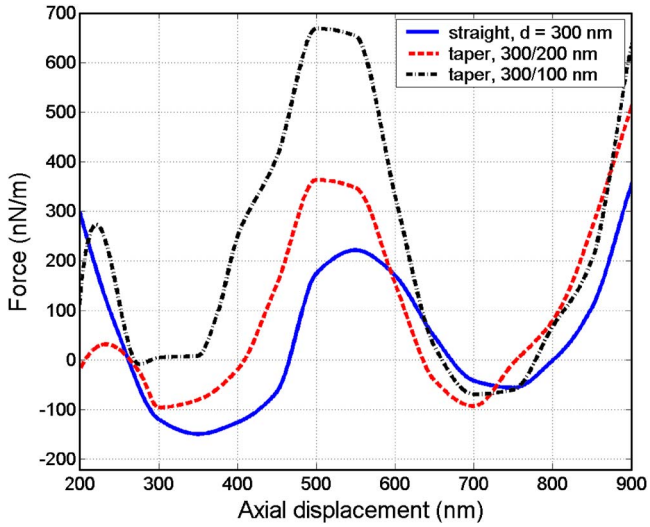

FIG. 8. (Color online) Axial net radiation force vs axial displacement for a 60 nm radius dielectric wire (n=1.3) illuminated by 400 nm TE cw laser source through rectangular and tapered slits.

wavelength is 1064 nm; the power is measured in the focal plane of objective; the numerical aperture is 1.3 and the amplification of the objective is 80×. The escape speed versus power dependence is measured by moving the laser beam by galvanometer controlled mirrors and finding the speed at which the bead escapes from the trap. In these measurements, we keep the position of the Gaussian beam waist at the same height h above the surface of the sample (the height of the trapped sphere above the surface is affected by the near fields of the gold pillars and changes during the scanning). The sample surface is found by speckle reflection of the trapping beam from the surface. This position is then set to 0 value of the z coordinate. The motorized z-drive was interferometrically calibrated before experiment. Also, we have the possibility to move the substrate by a motorized stage with a position resolution of 20 nm. The sample stage is used to achieve the initial rough positioning of the sample with respect to the laser beam with trapped particle. More details can be found in Ref. 30. The laser nanotrapping of

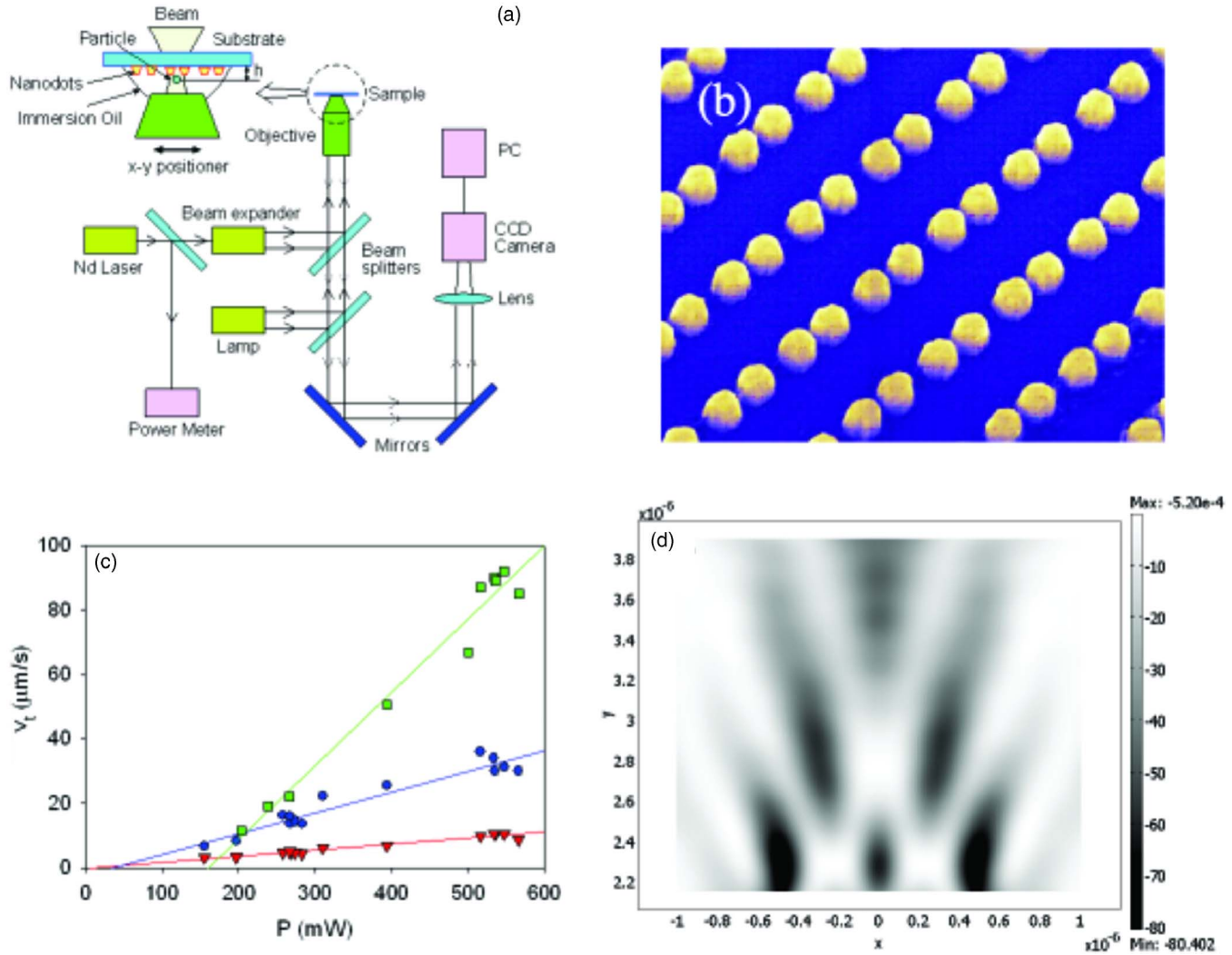

FIG. 9. (Color online) Experimental realization of laser nanotweezers based on nanostructured substrates. (a) Nanotweezer setup. (b) Scanning electron microscope micrograph of the array of gold nanodots on the glass substrate (the period of the array is 500 nm) used in the experiments in false colors. (c) The escape speed V_t of 1 μm dielectric beads at different heights h of the laser beam focus (Gaussian beam waist) from the sample as a function of laser power P: triangles—h=50 μm; circles—h=7 μm; and squares—h=3 μm. (d) Map of potential for the dipolar force of a 2D system consisting of three pairs of nanowires.

latex beads has been realized in immersion oil near the regular arrays of gold nanopillars arranged in pairs;[31] see Fig. 9(b).

The height of the nanopillars is 90 nm and the space between two adjacent nanopillars (in the pair) plays the role of the slit in the 2D apertured nanostructure described above. In this regard, it should be noted that while the nanopillar array is a 3D structure, its near-field trapping behavior is similar in some respects to that of our 2D structure. One such similarity is the significant increase in the trapping force near the nanostructured substrate for a given laser intensity. Moreover, our experiments showed that the resonances for 3D structures and for analogous 2D structures can be scaled. However, there exists a big difference between the distribution of the electromagnetic field for the aperture, which was theoretically studied, and the distribution of the field above the nanopillars (e.g., there exists a single equilibrium position for nanopillars and several of them for the aperture). Therefore, while it is obvious that our 2D results will not be in quantitative agreement with the 3D experimental work, we nevertheless introduce and discuss the latter because there are qualitative similarities between the trapping properties of the two systems. Specifically, for both the pillars and the aperture, the force enhancement is based on the localized plasmon resonances and, therefore, mostly depends on the surface charges generated near the aperture or at the surface of nanopillars and, hence, should be of the same order for two dimensions and three dimensions.

Figure 9(c) shows the escape speed of the dielectric beads of 1 μm size (we have analogous results for 200 nm beads) measured as a function of the power of the laser beam at different heights h of the trapping beam focus (Gaussian beam waist) above the surface of the sample. The escape speed was measured as the speed of the laser beam motion along the surface at which the bead becomes detached from the laser beam and is proportional to the maximal force exerted by laser beam on the bead. From Fig. 9(c), one can clearly see that the proximity of the nanostructured substrate significantly increases the escape speed of the 1 μm particle (v_t=9.8 μm/s at h=50 μm, 36 μm/s at h=7 μm, and 87 μm/s at h=3 μm at the laser power of 516 mW). The escape speeds of the order of 100 μm/s are very large and have never been observed for latex beads in immersion oil before. It should be noted here that despite aforementioned impossibility to compare 3D and 2D results, our simple 2D model can quantitatively (though roughly) back up this statement. An approximation to the force exerted on a sphere can be obtained by simply multiplying the force per unit length by the diameter of the sphere (in the Rayleigh limit of a small sphere). The force exerted on a 1 μm size latex particle in water estimated with the escape speed of 100 μm/s is equal to 1 pN. Because of the geometry of the experiment, this force corresponds to the lateral trapping force in our model that is equal to 3 fN when the radius of the particle is 60 nm. Since the dipolar force on a sphere scales as the cube of particle radius, the estimate of the force exerted on a 1 μm particle gives 1.7 pN, which is roughly comparable to the experimental value. It is also to be noted that almost an order of magnitude increase in the escape speed near the sample surface is observed despite a significant increase in the drag Stokes force one expects to have at such a small distance between the bead and the surface. This implies that the near fields of nanopillars produce at least an order of magnitude increase in the trapping force and, therefore, can be used to improve the trapping characteristics of the conventional laser tweezers. In Fig. 9(d), we show the results of a FEA of a 2D system that we study as a simplification of the 3D nanopillar structure. The 2D system consists of three pairs of tapered nanowires and each wire is 100 nm high with a base and top that are 100 and 70 nm wide, respectively. The two paired wires are separated by 50 nm and the separation between adjacent pairs is 200 nm at the base. The structure is illuminated with a TE 400 nm plane wave and a plot of the potential for the dipolar force indicates multiple distinct trapping regions, as was the case in our apertured structure [Fig. 9(d)].

V. SUMMARY

In summary, we have studied the near-field optical force on dielectric nanowires above subwavelength apertures in a planar plasmonic medium. We have found that the force changes sign with distance above the aperture and that there are positions at which a nanowire will be held in equilibrium. We have identified four factors that affect the equilibrium position: (i) the shape and the width of the slit, (ii) the wavelength of the incident light, (iii) the radius of the wire, and (iv) the dielectric properties of the wire. Our analysis indicates that nanostructured plasmonic media can be used for the controlled optical assembly or separation of subwavelength structures.

ACKNOWLEDGMENTS

The authors are grateful to Professor G. Schatz of Northwestern University for valuable discussions. This work was in part supported by a grant from the office of the Vice-President for Research at the University at Buffalo and in part by the Chemistry and Life Sciences Directorate of the Air Force Office of Scientific Research. The work in Manchester was supported by the Paul Instrument Grant.

[1] P. N. Prasad, *Nanophotonics* (Wiley, New York, 2004).
[2] A. Ashkin, in *Single Molecule Spectroscopy*, edited by R. Rigler, M. Orrit, and T. Basche (Springer, Berlin, 2002).
[3] S. Chu, Rev. Mod. Phys. **70**, 685 (1998).
[4] K. Svoboda and S. M. Block, Annu. Rev. Biophys. Biomol. Struct. **23**, 247 (1994).
[5] S. M. Block, Nature (London) **360**, 493 (1992).
[6] S. M. Block, Prog. Biophys. Mol. Biol. **65**, 21 (1996).
[7] C. Bustamante, J. C. Macosko, and G. J. L. Wuite, Nat. Rev. Mol. Cell Biol. **1**, 130 (2000).
[8] P. M. Hansen, V. K. Bhatia, N. Harrit, and L. Oddershede, Nano Lett. **5**, 1937 (2005).
[9] K. Okamoto and S. Kawata, Phys. Rev. Lett. **83**, 4534 (1999).
[10] E.-S. Kwak, T.-D. Onuta, D. Amarie, R. Potyrailo, B. Stein, S. C. Jacobson, W. L. Schaich, and B. Dragnea, J. Phys. Chem. B **108**, 13607 (2004).
[11] W. H. Choi, J. H. Jo, and S. Chang, J. Appl. Phys. **39**, 3961 (2000).
[12] L. Novotny, R. X. Bian, and X. S. Xie, Phys. Rev. Lett. **79**, 645 (1997).
[13] P. C. Chaumet, A. Rahmani, and M. Nieto-Vesperinas, Phys. Rev. Lett. **88**, 123601 (2002).
[14] M. Nieto-Vesperinas, P. C. Chaumet, and A. Rahmani, Philos. Trans. R. Soc. London, Ser. A **362**, 719 (2004).
[15] A. V. Zayats and I. I. Smolyaninov, J. Opt. A, Pure Appl. Opt. **5**, S16

(2003).
[16]K. Halterman, J. M. Elson, and S. Singh, Phys. Rev. B **72**, 075429 (2005).
[17]Sh.-H. Chang, S. K. Gray, and G. C. Schatz, Opt. Express **13**, 3150 (2005).
[18]K. L. Shuford, M. A. Ratner, S. K. Gray, and G. C. Schatz, J. Comput. Theor. Nanosci. **4**, 239 (2007).
[19]G. Volpe, R. Quidant, G. Badenes, and D. Petrov, Phys. Rev. Lett. **96**, 238101 (2006).
[20]S. Kawata and T. Tani, Opt. Lett. **21**, 1768 (1996).
[21]M. Righini, A. S. Zelenina, C. Girard, and R. Quidant, Nat. Phys. **3**, 477 (2007).
[22]L. A. Blanco and M. Nieto-Vesperinas, J. Opt. A, Pure Appl. Opt. **9**, S235 (2007).
[23]K. Dholakia, P. Reece, and M. Gu, Chem. Soc. Rev. **37**, 42 (2008).
[24]A. Vial, A.-S. Grimault, D. Macias, D. Barchiesi, and M. L. de la Chapelle, Phys. Rev. B **71**, 085416 (2005).
[25]See http://www.comsol.com/ for information about the COMSOL software.
[26]D. Zhang, X.-C. Yuan, S. C. Tjin, and S. Krishnan, Opt. Express **12**, 2220 (2004).
[27]R. C. Gauthier, Opt. Express **13**, 3703 (2005).
[28]W. Sun, S. Pan, and Y. Jiang, J. Mod. Opt. **53**, 2691 (2006).
[29]F. Zhou, X. Gan, W. Xu, and F. Gan, Opt. Express **14**, 12494 (2006).
[30]A. R. Sidorov, Y. Zhang, A. N. Grigorenko, and M. R. Dickinson, Opt. Commun. **278**, 439 (2007).
[31]A. N. Grigorenko, A. K. Geim, H. F. Gleeson, Y. Zhang, A. A. Firsov, I. Y. Khrushchev, and J. Petrovic, Nature (London) **438**, 335 (2005).